Available online at www.sciencedirect.com
SCIENCE DIRECT®
Journal of Solid State Chemistry 177 (2004) 4001–4006
JOURNAL OF SOLID STATE CHEMISTRY
www.elsevier.com/locate/jssc

Synthesis of Bi_2Se_3 thermoelectric nanosheets and nanotubes through hydrothermal co-reduction method

Hongmei Cui[a], Hong Liu[a,*], Xia Li[a], Jiyang Wang[a], Feng Han[a], Xudong Zhang[a], R.I. Boughton[b]

[a]*State Key Laboratory of Crystal Materials, Shandong University, 27 Shanda Nanlu, Jinan City, Shandong Province 250100, China*
[b]*Department of Physics and Astronomy, Bowling Green State University, Bowling Green, OH 43403, USA*

Received 16 March 2004; received in revised form 18 June 2004; accepted 24 June 2004
Available online 7 October 2004

Abstract

Bi_2Se_3 nanosheets and nanotubes were prepared by a hydrothermal co-reduction method at 150, 180, 200, and 210 °C. Bi_2Se_3 nanosheets, nanobelts and nanotubes were obtained. The Bi_2Se_3 nanoflakes are 50–500 nm in width and 2–5 nm in thickness. The Bi_2Se_3 nanotubes are 5–10 nm in diameter, 80–120 nm in length, and 1.3 nm in wall thickness. X-ray diffraction, transmission electron microscopy, high-resolution transmission electron microscopy, and electron diffraction were employed to characterize the products. Experimental results showed that the nanosheets and the nanotubes are hexagonal in structure with $a = 4.1354$ Å and $c = 27.4615$ Å. A possible formation and crystal growth mechanism of Bi_2Se_3 nanostructures is proposed.

Keywords: Bismuth selenide; Thermoelectric material; Nanotube; Hydrothermal Co-reduction

1. Introduction

Thermoelectric materials useful for thermoelectric cooling at room temperature and below have attracted much attention recently because of their potential applications in superconductors and electronic apparatus. Thermoelectric materials are ranked by a figure of merit, ZT, which is defined as $ZT = S^2\sigma T/\kappa$, where S is the thermopower or Seebeck coefficient [HN5], σ is the electrical conductivity, κ is the thermal conductivity, and T is the absolute temperature. To be competitive compared with conventional refrigerators and generators, one must develop materials with $ZT > 3$. Therefore, most work on thermoelectric materials focuses on improving the figure of merit. Although several new thermoelectric materials possessing much better properties than conventional materials have been developed, such as filled Skutterudites [1], $CsBi_4Te_6$ [2], half-Heusler alloys [3], intermetallic clathrates [4,5], the efficiency of thermoelectric generators prepared from such materials is still too low to be suitable for widespread application. Recently, thermoelectric nanostructures, quantum wells, quantum wires and quantum dots, have been proven to have much higher thermoelectric coefficients than bulk materials according to both theoretical and experimental investigations [6–9]. The compound $(Bi,Sb)_2(Se,Te)_3$ has been extensively investigated during the past 40 years because of its good thermoelectric cooling at room temperature and its high ZT [10,11]. In order to obtain advanced thermoelectric materials, several groups have prepared $(Bi,Sb)_2(Se,Te)_3$ films with a quantum well structure by sputtering or other physical methods [1,12]. During the past decade, low-cost, timesaving wet-chemical methods have been used to synthesize some nanostructures, such as films, nanorods, nanowires and nanobelts of oxides, metals, alloys, and other compounds [13–16]. Up to now, there has been little work on the synthesis of thermoelectric

*Corresponding author. Fax: +86-531-857-4135.
E-mail addresses: hongliu@sdu.edu.cn (H. Liu), jywang@icm.sdu.edu.cn (J. Wang).

0022-4596/$ - see front matter © 2004 Published by Elsevier Inc.
doi:10.1016/j.jssc.2004.06.042

material nanostructures by wet-chemical methods. Previously our group synthesized skutterudite nanowires for thermoelectric applications [17,18]. Sander et al. [19] have reported an electro-deposition method for the synthesis of Bi_2Te_3 nanowires by using porous anodic alumina templates. Recently, Ding et al. [20–22] and Qian's group synthesized Sb_2Se_3 nanowires and Bi_2Se_3 nanoflakes through a solvothermal reaction [20]. In this paper, we report that Bi_2Se_3 nanostructures have been synthesized by a hydrothermal co-reduction method. The powder product synthesized at low temperature consists mainly of Bi_2Se_3 nanoflakes. Some nanotubes have been found among the nanoflakes in the powder product synthesized at higher temperatures.

2. Experimental section

For preparing Bi_2Se_3, 7.5 mL of H_2SeO_3 solution (1 mol/L) was put into a Teflon-lined autoclave of 25 mL capacity. 0.005 mol of $BiCl_3$ was added into the H_2SeO_3 solution. After ultrasonic agitation for about 30 min, 4 mL of hydrazine hydrate ($N_2H_4 \cdot H_2O$) was poured into the reactants. The autoclave was filled with deionized water up to 80% of the total volume, sealed, and heated at 150, 180 and 200 and 210 °C for 24 h in an electric furnace. After heating, the system was cooled down to room temperature naturally. The black-colored product that was obtained (the yield is about 95%) was collected by filtration, washed with deionized water and absolute ethanol, and then dried at 60 °C in a vacuum drier.

The samples obtained were characterized by X-ray diffraction (XRD) on a D max-γ A model (Japan Rigaku) XRD system with Ni-filtered Cu$K\alpha$ radiation ($\lambda = 1.5059$ Å). The size and morphology of the particles of the powder product were determined by a Hitachi model H-800 transmission electron microscope (TEM) and a Philips Tecnai 20v-Twin high-resolution transmission electron microscope (HRTEM). Samples for the TEM and HRTEM were prepared by ultrasonically dispersing the as-synthesized Bi_2Se_3 products into absolute ethanol, then placing a drop of this suspension onto a copper grid coated with an amorphous carbon film and then drying in air.

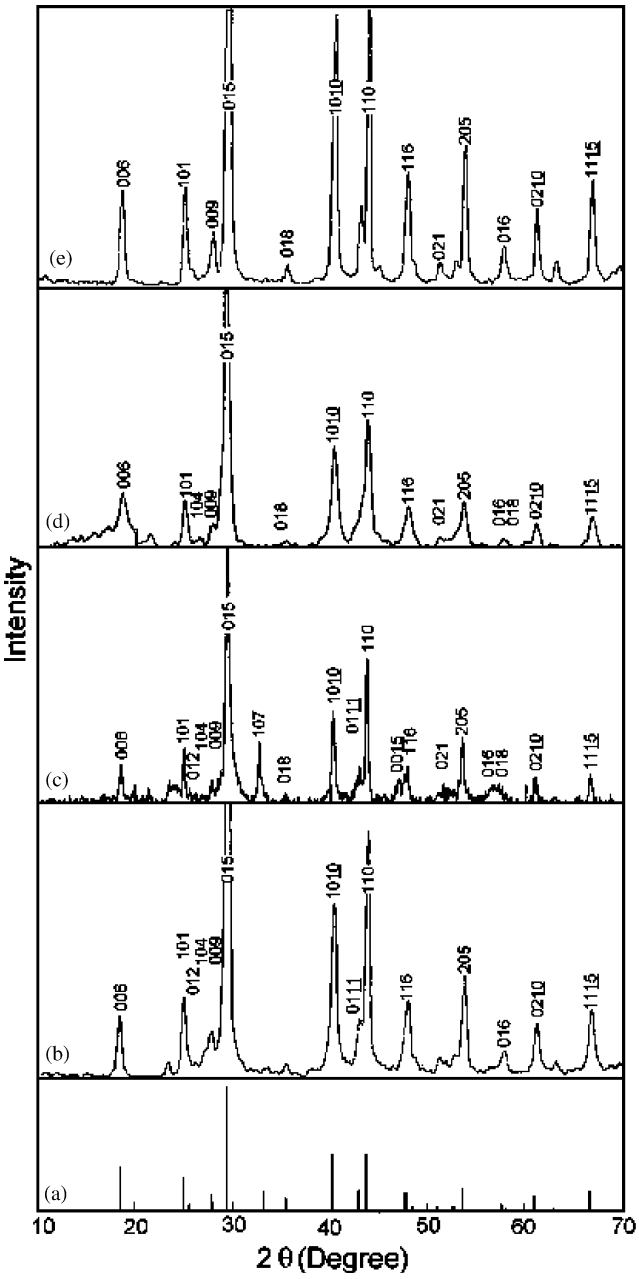

Fig. 1. XRD patterns of powder products synthesized by hydrothermal co-reduction method: (a) standard pattern, (b) synthesized at 150 °C for 24 h, (c) synthesized at 180 °C for 24 h, (d) synthesized at 200 °C for 24 h, and (e) synthesized at 210 °C for 24 h.

3. Results and discussion

Fig. 1(a–e) shows the XRD patterns of Bi_2Se_3 (JCPDS 33-214), the powder product obtained at 150, 180, 200 and at 210 °C for 24 h, respectively. All the diffraction peaks in the patterns of all the product powders correspond to the peaks of hexagonal Bi_2Se_3 (JCPDS 33-214) with space group: $R\bar{3}m$ (166). Peaks for bismuth, selenium or other bismuth–selenium compounds do not appear in the diffraction pattern. The cell parameters calculated from the XRD pattern are $a = 4.1354$ Å and $c = 28.4615$ Å, which are consistent with the cell parameters in JCPDS 33-214, $a = 4.1396$ Å, and $c = 28.636$ Å. Therefore, the product powder obtained is hexagonal Bi_2Se_3.

Fig. 2 shows TEM images of the product powders synthesized at 150 °C for 24 h. We observed that most particles are thin hexagonal nanosheets of diameter between 50 and 100 nm in this case. Among the

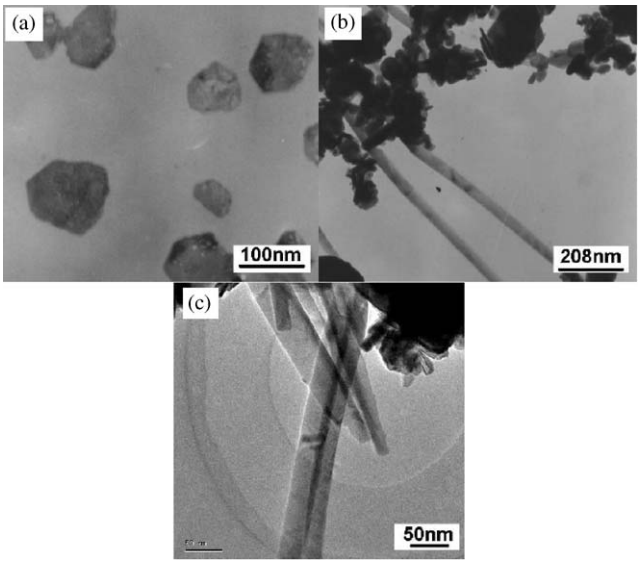

Fig. 2. TEM images of powder products synthesized at 150 °C for 24 h: (a) TEM images of bismuth selenide hexagonal nanosheets, (b) and (c) TEM images of the synthesized bismuth selenide nanobelts.

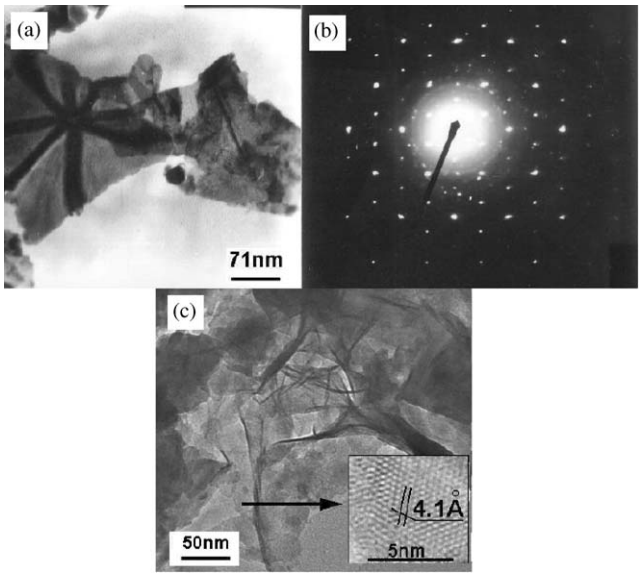

Fig. 3. TEM and HRTEM images of powder product synthesized at 180 °C for 24 h: (a) TEM image of nanoflakes, (b) ED pattern of normal to a nanoflake, and (c) HRTEM image of the nanoflake; inset, lattice image of the nanoflake.

particles, there are some nanobelts 20–50 nm in breadth and more than 1000 nm in length (Fig. 2b and c).

Fig. 3a shows the TEM images of the product powder synthesized at 180° C for 24 h. The particles synthesized at 180° C are very thin nanosheets with irregular morphology about 200–500 nm in dimension. Fig. 3b shows the electron diffraction (ED) pattern normal to the plane of a sheet. It indicates that the nanosheets are well crystallized and grow along the (0001) face. The cell parameter a calculated from the ED pattern is 4.12 Å, which is close to the result calculated from the XRD pattern and the parameter provided in the Diffraction Card (33-214). Fig. 3c shows a high-resolution electron microscope image of the sheets. From the kinked parts of the sheets, we can see that the thickness of the flakes is about 5–10 nm. The inset of Fig. 3c is the HRTEM image recorded near the edge of a nanosheet. The lattice image has hexagonal symmetry, which is more evidence in support of the suggestion that the Bi_2Se_3 nanosheet grows along the (0001) plane. The HRTEM pattern shows a well-resolved interference fringe spacing of 0.41 nm that agrees well with twice the interplanar distance between the 110 lattice planes ($d_{110} = 2.027$ Å in the XRD pattern, $d_{110} = 2.07$ Å on the powder XRD card 33-214).

Fig. 4 shows the TEM and HRTEM images of the powder product synthesized at 200 °C for 24 h. From the TEM observation, we found that there are still some nanosheets in the product. Among the nanosheets, some nanotubes 10–20 nm in diameter can be found. Fig. 4a shows that six nanotubes connect to form a dendrite. Fig. 4b shows the nanotubes with higher resolution under HRTEM. The measured wall thickness of the

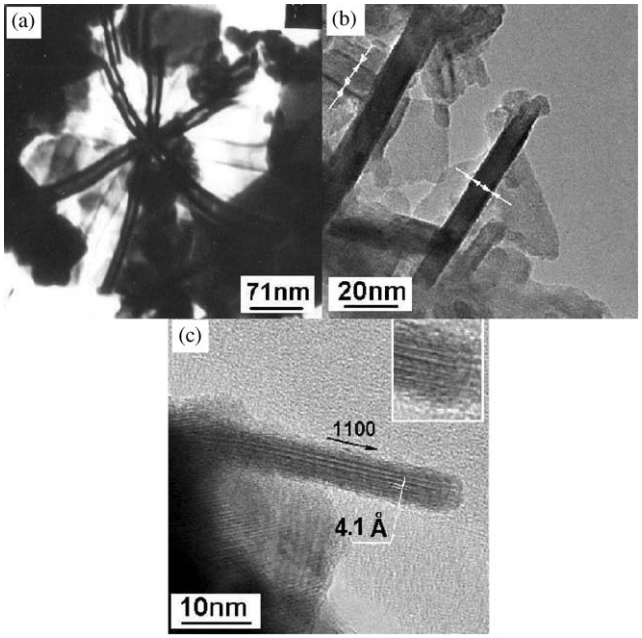

Fig. 4. HRTEM of powder product synthesized at 200 °C for 24 h: (a) nanotubes, (b) lattice image of a nanotube, (c) the mixture of nanotubes and amorphous nanopaticles, and (d) a nanotube connects with a bulb-like particle on one end.

nanotubes is about 1.3 nm. Fig. 4c shows the HRTEM image of a nanotube. From Fig. 4c, we can see that the nanotube is about 5 nm in diameter, and 40 nm in length. At the top of the tube, we can see the opening of the tube clearly. The measured thickness of the tube wall at the top of the tube is also about 1.3 nm, which is close

to the thickness of a $Se^{(1)}$–Bi–$Se^{(2)}$–Bi–$Se^{(1)}$ multi-layer unit, 13.8207 Å, a half cell parameter, c. From the lattice image of the nanotube, we obtain the measured distance between the two lines to be about 4.1 Å, which is also close to twice the interplanar distance between the 110 lattice planes ($d_{110} = 2.027$ Å in the XRD pattern, $d_{110} = 2.07$ Å on the powder XRD card 33-214). Therefore, we conclude that the structure of Bi_2Se_3 nanotubes is similar to multi-layered carbon nanotubes. The tube wall is multilayered, that is, a $Se^{(1)}$–Bi–$Se^{(2)}$ multilayer. From the above evidence, we assume that the Bi_2Se_3 nanotubes grow along the [1100] direction, and the tubes form by the bending of the (0001) plane to form a butt joint.

Fig. 5 shows the TEM images of the product synthesized at 210 °C for 24 h. Most of the particles in the product are large well-crystallized hexagonal sheets, and most of them are larger than 300 nm in dimension (Fig. 5a). From the TEM image, we can see that the sheets synthesized at 210 °C are much thicker than that of the product synthesized at 180 or 200 °C. In the product, some wire-like nanostructures can be found. Fig. 5b shows a wire-like particle in the product. From the figure, we can see that the particle is apparently not a nanotube, but is a long belt bending in the width direction (insert of Fig. 5b).

According to all the above evidences, we can suggest a formation mechanism of the nanosheets and nonotubes.

When all the reactants are put into the autoclave and heated, Bi^{3+} atoms and Se^{4+} are reduced by NH_2–NH_2:

$$H_2SeO_3 + N_2H_4 \cdot H_2O \rightarrow Se + N_2 \uparrow + 4H_2O, \quad (1)$$

$$4BiCl_3 + 3N_2H_4 \rightarrow 4Bi + 3N_2 \uparrow + 12HCl. \quad (2)$$

Because the electrode potential of both bismuth with a valence of +3 and selenium with valences of +4 to zero are positive,

$$BiOCl + 2H^+ + 3e^- \rightarrow Bi + H_2O + Cl^- + 0.16\,V, \quad (3)$$

$$H_2SeO_3 + 4H^+ + 4e^- \rightarrow Se + 3H_2O + 0.74\,V. \quad (4)$$

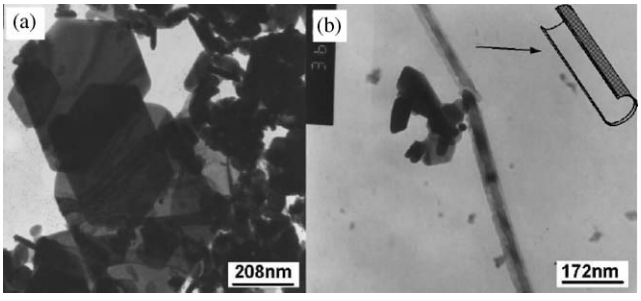

Fig. 5. The TEM images of the product synthesized at 210 °C for 24 h: (a) large well-crystallized hexagonal sheets, and (b) wire-like nanostructures; inset shows the schematic depiction of the formation of Bi_2Se_3 belt bending in the width direction.

Both of them are easily reduced by N_2H_4. Bi and Se easily compound to form Bi_2Se_3, because both the as-reduced Bi and Se are active.

$$2Bi + 3Se \rightarrow Bi_2Se_3. \quad (5)$$

When the Bi_2Se_3 molecules accumulate, and their concentration of Bi_2Se_3 in the solution is high enough, Bi_2Se_3 crystal nuclei form.

Fig. 6 shows the crystal structure of hexagonal Bi_2Se_3 [14]. The crystal structure of Bi_2Se_3 consists of Bi and Se layers. A Bi layer is made up of Bi atoms arranged to form a plane hexagonal structure, and a Se layer is formed by Se atoms arranged in the same way. As shown in Fig. 6, in a unit cell, there are two different types of Se layers, named $Se^{(1)}$ and $Se^{(2)}$. The unit cell is packed with two Bi layers and three Se layers following the pattern: $Se^{(1)}$–Bi–$Se^{(2)}$–Bi–$Se^{(1)}$. Between two units, there is only the Van der Waals bond between the neighboring $Se^{(1)}$ planes. Therefore, the crystal cleaves easily between the $Se^{(1)}$ planes.

To explain the growth mechanism of the Bi_2Se_3 nanostructure synthesized at different temperatures, a suggested schematic model is shown in Fig. 7.

Because Bi_2Se_3 has a special layered structure and weak bonds between two unit layers unite (Fig. 6), the nuclei forming from the solution are tiny thin crystals (Fig. 7a-1). When the reaction temperature is low, the formation rate of Bi_2Se_3 molecules and the growth rate of the crystal are low. It is easy to get small crystalline nanosheets with well-formed hexagonal morphology (Fig. 7a-2). For this reason, most of the particles in the product synthesized at 150 °C for 24 h are hexagonal

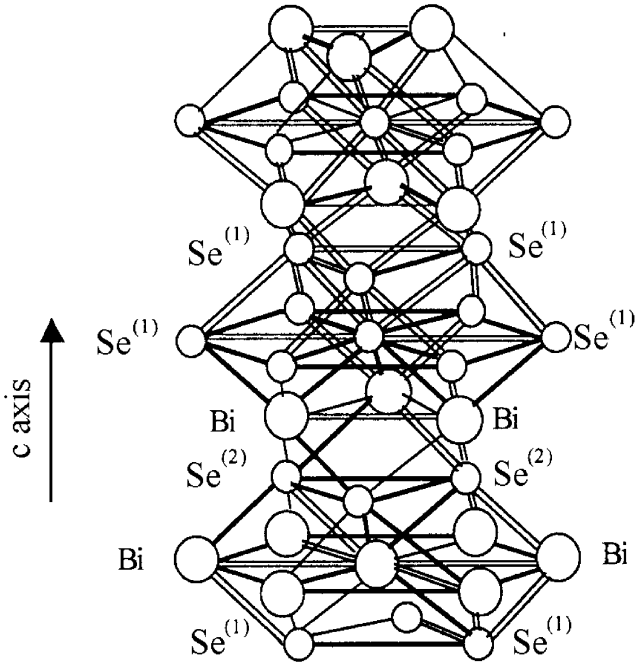

Fig. 6. Crystal structure of hexagonal Bi_2Se_3.

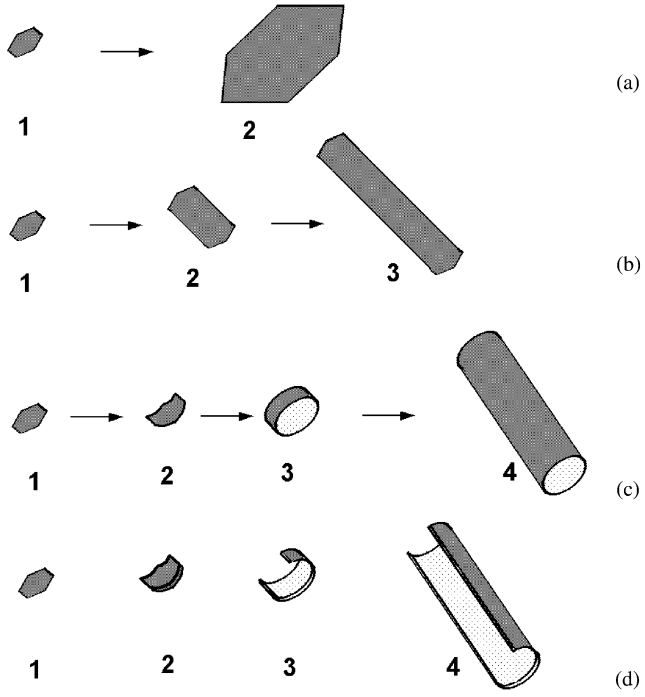

Fig. 7. The schematic depiction of the formation of Bi_2Se_3 nanostructures.

nanocrystals. For some nuclei in the solution, the crystal grows along the [110] direction (Fig. 7b-2), and forms a nanobelt (Fig. 7b-3).

The size of nanoflakes increases with increasing the heating temperature. When the heating temperature is 180 °C, despite the increasing size of nanoflakes, no other special phenomenon appears. When the heating temperature is further increased, the formation rate of Bi_2Se_3 in the reactants solution apparently increases. Because the system is in a high-energy-state, some defects should form in the nuclei during the nucleation. The defects cause the bending of the nuclei (Fig. 7c-2). As the crystal growth continues, the bending nuclei grows into a ring (Fig. 7c-3). With increasing heating time, the ring grows along its axis, and then forms a long nanotube.

When the heating temperature is over 200 °C, the rate of formation of Bi_2Se_3 molecules and the growth of Bi_2Se_3 crystals are very high. When the nuclei form from the solution, Bi_2Se_3 molecules easily grow epitaxially on the surface of thin nuclii and form new layers of Bi_2Se_3. In this situation, although bending nuclei with defects can form in the solution (Fig. 7d-2), It is difficult for them to bend into rings, rather they can only forms short arcs (Fig. 7d-3), because the nuclei are too thick. With increase in the heating time at this temperature, the arc crystals grow into long belts bending along the breadth direction (Fig. 7d-4). The existence of bending belts in the product synthesized at 210 °C for 24 h supports our proposed mechanism of Be_2Se_3 nanotubes.

The growth mechanism of Bi_2Se_3 nanotubes is different from the formation of tellurium nanobelts synthesized through the hydrothermal method by Mu et al. [21]. In their work, they demonstrated that the tellurium nanotubes grew from Tellurium nanobelts, and that the growth mechanism is based on a helical belt template mechanism. In our work, we have not found helix nanobelts in the same product.

As mentioned above, Bi_2Se_3 is a typical thermoelectric material with excellent thermoelectric properties. Bi_2Se_3 nanotubes synthesized through this low-cost method can potentially be used for the preparation of thermoelectric nanostructures or quantum devices by chemical self-assembly.

4. Conclusions

Bi_2Se_3 nanoflakes and nanotubes are synthesized through a hydrothermal co-reduction method. XRD measurement proves that Bi_2Se_3 nanoflakes and nanotubes are hexagonal bismuth selenide with lattice parameters $a = 4.1354$ Å and $c = 27.4615$ Å. The results of ED and HRTEM support the lattice parameter values calculated from XRD. TEM and HRTEM observation indicate that the nanoflakes synthesized at 150–210 °C are 50–500 nm in width, and 2–5 nm in thickness, and the size and thickness of the nanoflakes increase with increase heating temperature. The Bi_2Se_3 nanotubes are 5–20 nm in diameter, 80–120 nm in length, and 1.3 nm in wall thickness. The Bi_2Se_3 compound is obtained from the compound reaction of bismuth and selenium from the co-reduction of Bi^{3+} and Se^{4+}. The Bi_2Se_3 nanoflakes grow along the (001) plane. Bi_2Se_3 nanotubes grow along the [1100] direction, and the tubes form by the bending of the (0001) planes to form a butt joint. The Bi_2Se_3 nanotubles grow from bending nuclei. A detailed formation model of Bi_2Se_3 nanosheets, nanotubes, and nanobending belts is suggested.

Acknowledgements

This work was supported by the National High Technology Research and Development Program of China (863 program, No. 2002AA311110), the Natural Science Foundation of China (Grant No. 60025409), Young Scientists Award Fund of Shandong Province, and the Grant of State Key Program of China.

References

[1] B.C. Sales, D. Madrus, R.K. Willianms, Science 272 (1996) 1325–1328.

[2] D.-Y. Chung, T. Hogan, P. Brazis, M. Rocci-Lane, C. Kannewurf, M. Bastea, C. Uher, M.G. Kanatzidis, Science 287 (2000) 1024–1027.
[3] S.J. Poon, Semicond. Semimet. 70 (2001) 37.
[4] I. Terasaki, et al., Jpn. J. Appl. Phys. 40 (2001) L65.
[5] G.S. Nolas, G. A Slack, S.B. Schujman, Semicond. Semimet. 69 (2001) 255.
[6] B.C. Sales, Science 295 (2002) 1248.
[7] M.S. Sander, A.L. Prieto, H.Z. Kou, T. Sands, A.M. Stacy, Adv. Mater. 14 (2002) 665.
[8] L.D. Hicks, M.S. Dresselhaus, Phys. Rev. B. 47 (1993) 12.
[9] K.F. Hsu, S. Loo, F. Guo, W. Chen, J.S. Dyck, C. Uher, T. Hogan, E.K. Polychroniadis, M.G. Kanatzidis, Science 303 (2004) 818.
[10] T.M. Tritt, Science 283 (1999) 804.
[11] R. Venkatasubramanian, E. Siilvola, T. Colpitts, B. O'Quinn, Nature 413 (2001) 597.
[12] T.C. Harman, P.J. Taylor, M.P. Walsh, B.E. LaForge, Science 297 (2002) 2229.
[13] Maosong Mo, Jinghui Zeng, Xianming Liu, Weichao Yu, Sshuyuan Zhang, Yitai Qian, Adv. Mater. 14 (2002) 1658.
[14] Qing Peng, Yajie Dong, Zhaoxiang Deng, Yadong Li, Inorg. Chem. 41 (2002) 5249.
[15] Yuan-Tao Chen, Jing-Bo Ding, Mater. Chem. Phys. 77 (2002) 734.
[16] ZhengPing Qiao, Gang Xie, J. Solid State Chem. 166 (2002) 49.
[17] H. Liu, J.Y. Wang, X.B. Hu, F. Gu, L. Hua, C.Q. Zhang, B. Teng, Chem. Mater. 13 (2001) 151.
[18] Hong Liu, Jiyang Wang, Xiaobo Hu, Lixia Li, Feng Gu, Shanrong Zhao, Mingyuan Gu, R.I. Boughton, Minhua, Jiang, J. Alloys Compd. 334 (2002) 313.
[19] M.S. Sander, A.L. Prieto, H.Z. Kou, T. Sands, A.M. Stacy, Adv. Mater. 14 (2002) 665.
[20] Z. Ding, L. Viculis, J. Nakawatase, R.B. Kaner, Intercalation and solution processing of bismuth telluride and bismuth selenide, Adv. Mater. 13 (2001) 797.
[21] Debao Wang, Dabin Yu, Maosong Mo, Xianming Liu, Yitai Qian, J. Crystal Growth 253 (2003) 445–451.
[22] Maosong Mo, Jianghui Zeng, Xianming Liu, Weichao Yu, Shuyuan Zhang, Yitai Qian, Adv. Mater. 14 (2002) 1658.